Theory and computation of higher gradient elasticity theories based on action principles

B. Emek Abali [*†]   Wolfgang H. Müller [‡]   Francesco dell'Isola [§]

Abstract

In continuum mechanics there exists a unique theory for elasticity, which includes the first gradient of displacement. The corresponding generalization of elasticity is referred to as *strain gradient elasticity* or *higher gradient theories*, where the second and higher gradients of displacement are involved. Unfortunately, there is a lack of consensus among scientists how to achieve the generalization. Various suggestions were made, in order to compare or even verify these, we need a generic computational tool. In this paper we follow an unusual but quite convenient way of formulation based on action principles. First, in order to present its benefits, we start with the action principle leading to the well-known form of elasticity theory and present a variational formulation in order to obtain a weak form. Second, we generalize elasticity and point out, in which term the suggested formalism differs. By using the same approach we obtain a weak form for strain gradient elasticity. The weak forms for elasticity and for strain gradient elasticity are solved numerically by using open-source packages—by using the finite element method in space and finite difference method in time. We present some applications from elasticity as well as strain gradient elasticity and simulate the so-called size-effect.

1. Introduction

Starting with works Joseph-Louis de Lagrange, Pierre Louis Moreau de Maupertius, Leonhard Euler—for a short history see Romano et al. (2009)—the theory of mechanics is formulated by an energy expression called LAGRANGEan that depends on primitive variables and their *first* derivatives in coordinates. Such a theory is of first order since the first derivative in coordinates describes the immediate neighborhood. This is an infinitesimally small region given by a sphere of radius ε. In continuum mechanics we declare the size of ε as approaching zero. Therefore, from a conceptual point of view, no problems arise and continuum mechanics is sufficient to characterize the immediate neighborhood with the first derivative. This approach is also called the locality argumentation and is valid for analytical mechanics, where we can set ε infinitesimally small. However, if we want to exploit numerical mechanics, then we have to set a finite value for ε. It has to be smaller than the *length-scale* of the underlying structure.

In order to explain the length-scale, consider a measurement where the machine precision is limited to $1\,\mu m$. Therefore, we simply miss any deformation occurring on a smaller scale than a micrometer length-scale. We have to choose ε smaller than $1\,\mu m$ and then we can accurately model the measurement. Moreover, we set ε large enough such that sufficiently many atoms are included, so we may ignore any fluctuation effects. Suppose

---

[*]Corresponding author, email: b.e.abali@berkeley.edu
[†]University of California, Berkeley
  Department of Mechanical Engineering
  6124 Etcheverry Hall, Mailstop 1740, Berkeley, CA 94720, USA
[‡]Technische Universität Berlin
  Institute of Mechanics
  Chair of Continuum Mechanics and Theory of Materials
  Einsteinufer 5, 10587, Berlin, Germany
[§]Sapienza Universita di Roma
  Dipartimento di Ingegneria Strutturale e Geotecnica
  Via Eudossiana 18, 00184, Roma, Italia

we can estimate 1 nm as the minimum size of ε, i.e., for a monatomic lattice we assume that first neighbor is in a distance less than 1 nm. In a smaller length-scale the atomistic structure and interactions between lattice points become important. Between 1 nm and 1 μm the size of ε can be chosen arbitrarily, the solution of the problem remains the same, for the idea of self-similarity and intermediate distances see Barenblatt (1996, Chap. 2). The first order theory holds accurately for a material point in the given length-scale, i.e., ε is smaller than the upper limit of 1 μm and greater than the lower limit of 1 nm. We can measure with a measurement device capturing 1 μm and model the measurement with the first order theory.

Now consider a material with 1 μm grain size. In other words, the underlying material has a substructure within the length-scale. Now we have two different options to resolve this issue. Either we redeclare the length-scale by decreasing the upper limit, simply stated, we buy a new measurement device with a higher precision; or we generalize the first order theory in order to capture the effects of the substructure. This generalization introduces *new* coefficients responsible for the response effected by the substructure. In this work we explain the method of least action and exploit it for generalizing the continuum theory from the first order to the second order.

Although the idea of an extended or generalized mechanics is older than a century, see dell'Isola et al. (2014), the modern theory started to be developed by the early 1960s with Mindlin and Tiersten (1962), Mindlin (1964), Toupin (1964), Eringen (1967). Today there are various theories describing an extension of the first order theory for elasticity. Interestingly, these different theories are mathematically quite similar and can be viewed as specialized versions of a unified theory, see Neff et al. (2014). By starting with experimental evidence as in Morrison (1939) and then later on in Yang and Lakes (1982), Brezny and Green (1990), Chen and Fleck (2002), Kesler and Gibson (2002), we know that a second order theory—called the strain gradient theory—is necessary for an accurate prediction of experiments. For example, the prominent experiment of beam bending can be investigated. Consider a beam of 1 μm length and another beam of 1 mm, both out of the same material. The first order theory is accurate for the beam in the meter length-scale; however, it is inaccurate for the beam in the micrometer length-scale. Apparently, for the micrometer beam, the substructure of the material becomes dominant. An internal substructure can be a crystallographic structure of aluminum or polymer chains of epoxy. If one wants to acquire accurate results with the first order theory then a precise and detailed model of this substructure needs to be involved. However, this method is not efficient at all. In other words, although we might try to model everything by molecular dynamics, we never do that for a structure bigger than a couple of micrometers due to the computational time required for such a detailed model. We will present a second order theory, capable of modeling the deformation of beam bending even on smaller length-scales, with an adequate amount of computational cost.

Computational issues of generalized mechanics are heavily discussed in the literature. There are various propositions and numerical strategies. For example Bilotta et al. (2010) uses a promising method by constructing special elements. The newly introduced material parameters can be motivated with a rigorous micro-macro identification procedure, see Pideri and Seppecher (1997). Based on this idea, Giorgio (2016) provides a persuasive series of numerical results, starting from the first order theory. In various applications, effects of substructure are unavoidable, for simulations of interesting examples, see Scerrato et al. (2016), Turco et al. (2016), and Placidi et al. (2015). Finite element implementation and comparable results to the underlying work have appeared recently in Reiher et al. (2016). We present our formulation and its implementation in a quite general setting, hence an extension to many other branches than elasticity is possible. For example, the numerical solution procedure presented herein seems to be potentially very useful also for studying the equilibrium problems of second gradient fluids as discussed in Eremeyev (2016), Eremeyev and Altenbach (2014).

First we discuss the variational formulation in the first order theory by means of an action principle. Instead of the least action principle, another similar theory known as principle of virtual work (or power) can be used, too. We start by postulating an action and omit to give its detailed form. If a principle of virtual work needs to be used, then we immediately have to describe the form. There are no big discrepancies between these methods. Second, we generalize the variational formulation for the second order theory by following Abali and Müller (2016). The outcome is a weak form necessary for the computation. Third, we present a numerical tool solving the weak form. For the case of elasticity and strain gradient elasticity, we perform several simulations in order to justify the benefits of the approach. We use open-source packages and make our codes publicly available in order to encourage further studies.

2. Variational formulation for the first order theory

The general formulation relies on a mathematical construct called *action*. The first postulate in this methodology is an existing LAGRANGEan density, $\mathcal{L}$, describing the underlying system

$$\mathcal{L} = \mathcal{L}\left(x_\mu, \phi_A, \phi_{A,\mu}\right) , \quad \phi_{A,\mu} = \frac{\partial \phi_A}{\partial x_\mu} , \tag{1}$$

which depends on Cartesian coordinates, $x_\mu \in \Omega$, $\mu = 1, 2, \ldots m$, in m-th dimensional space, $\Omega \subset \mathbb{R}^m$; on primitive variables, $\phi_A = \phi_A(x_\mu)$; as well as on their derivatives, $\phi_{A,\mu} = \phi_{A,\mu}(x_\mu)$. Only the first derivatives are included in the list of arguments. The LAGRANGEan density describes the *state* of the underlying system. Thus, we call $\{\phi_A, \phi_{A,\mu}\}$ the *state space*. Consider a continuum body defined in the space $x_\mu = (t, x, y, z)$ is being deformed under a given mechanical loading. Then the state is the deformation of the body defined by the displacement field, $\phi_A = u_i = u_i(t, x, y, z)$, and its first gradient in coordinates. The space spanned by the displacement field and its first gradient in coordinates creates the state space. This concept is often used in terms of rigid bodies, where the displacement and velocity (derivative in t) create the state space.

The second postulate is the so-called action functional:

$$\mathcal{A} = \int_\Omega \mathcal{L} \, \mathrm{d}\Sigma + \int_{\partial\Omega} W_\mathrm{s} \, \mathrm{d}\Gamma , \quad \mathrm{d}\Sigma = \mathrm{d}x_1 \, \mathrm{d}x_2 \ldots \mathrm{d}x_m , \quad \mathrm{d}\Gamma = \mathrm{d}x_1 \, \mathrm{d}x_2 \ldots \mathrm{d}x_{m-1} , \tag{2}$$

where we have used the Cartesian coordinates such that the metric determinant of the space Ω is equal to 1. If we call $\mathrm{d}\Omega$ an infinitesimal *volume* element, then one dimension less $\mathrm{d}\Omega$ would be a *surface* element. We have a first order theory such that only one dimension lower space is included. Technically, we know W_s on the surface and want to determine the appropriate $\mathcal{L}$ within the space. Thus, W_s is given and we restrict it be depending on ϕ_A. The action is a scalar, i.e., it is invariant with respect to the transformation of primitive variables. First we introduce variations of the primitive variables,

$$\phi'_A = \phi_A + \varepsilon\delta\phi_A , \tag{3}$$

and of its rates,

$$\phi'_{A,\mu} = \phi_{A,\mu} + \varepsilon\delta\phi_{A,\mu} , \quad \delta\phi_{A,\mu} = (\delta\phi_A)_{,\mu} = \frac{\partial\delta\phi_A}{\partial x_\mu} . \tag{4}$$

The test functions, $\delta\phi_A$, are arbitrary; however, they are chosen to vanish on the DIRICHLET boundaries, $\partial\Omega_\mathrm{D}$, where the primitive variables are known. The constant factor ε is such a small number (with respect to the upper limit in the length-scale) that the above transformation is accurate in the first order in ε. Now, with the same accuracy, the variation of the action reads

$$\delta\mathcal{A} = \int_\Omega \mathcal{L}' \, \mathrm{d}\Sigma - \int_\Omega \mathcal{L} \, \mathrm{d}\Sigma + \int_{\partial\Omega} W'_\mathrm{s} \, \mathrm{d}\Gamma - \int_{\partial\Omega} W_\mathrm{s} \, \mathrm{d}\Gamma , \quad \mathcal{L}' = \mathcal{L}\left(x_\mu, \phi'_A, \phi'_{A,\mu}\right) , \quad W'_\mathrm{s} = W_\mathrm{s}\left(x_\mu, \phi'_A\right) . \tag{5}$$

By using a TAYLOR expansion linear in ε we obtain

$$\mathcal{L}' = \mathcal{L}\left(x_\mu, \phi'_A, \frac{\partial\phi'_A}{\partial x_\mu}\right) = \mathcal{L}\left(x_\mu, \phi_A, \phi_{A,\mu}\right) + \frac{\partial\mathcal{L}\left(x_\mu, \phi_A, \phi_{A,\mu}\right)}{\partial\phi_A}(\phi'_A - \phi_A) + \frac{\partial\mathcal{L}\left(x_\mu, \phi_A, \phi_{A,\mu}\right)}{\partial\phi_{A,\mu}}(\phi'_{A,\mu} - \phi_{A,\mu}) =$$

$$= \mathcal{L} + \frac{\partial\mathcal{L}}{\partial\phi_A}\varepsilon\delta\phi_A + \frac{\partial\mathcal{L}}{\partial\phi_{A,\mu}}\varepsilon\delta\phi_{A,\mu} , \tag{6}$$

and analogously,

$$W'_\mathrm{s} = W_\mathrm{s} + \frac{\partial W_\mathrm{s}}{\partial\phi_A}\varepsilon\delta\phi_A , \tag{7}$$

where and henceforth over repeated indices we apply the EINSTEIN summation convention. The variation of action becomes

$$\delta\mathcal{A} = \int_\Omega \left(\frac{\partial\mathcal{L}}{\partial\phi_A}\varepsilon\delta\phi_A + \frac{\partial\mathcal{L}}{\partial\phi_{A,\mu}}\varepsilon\delta\phi_{A,\mu}\right)\mathrm{d}\Sigma + \int_{\partial\Omega} \frac{\partial W_\mathrm{s}}{\partial\phi_A}\varepsilon\delta\phi_A \, \mathrm{d}\Gamma . \tag{8}$$

According to the *principle of least action* the action functional is a scalar such that its variation vanishes

$$\delta\mathcal{A} = 0 , \tag{9}$$

for non-dissipative (reversible) systems. Since ε is a constant non-zero number, we can divide by it such that we obtain

$$\int_{\Omega} \left(\frac{\partial \mathcal{L}}{\partial \phi_A} \delta \phi_A + \frac{\partial \mathcal{L}}{\partial \phi_{A,\mu}} \delta \phi_{A,\mu} \right) \mathrm{d}\Sigma + \int_{\partial \Omega} \frac{\partial W_{\mathrm{s}}}{\partial \phi_A} \delta \phi_A \, \mathrm{d}\Gamma = 0 \ . \tag{10}$$

This integral form is general for a system having a LAGRANGEan density depending on the primitive variables and their first derivatives. Often, an integration by parts is established on the second term within Σ such that the integrand contains only $\delta \phi_A$. This step introduces a surface integral derived from $\mathcal{L}$ set in with $\partial W_{\mathrm{s}}/\partial \phi_A$. Within Σ the so-called EULER–LAGRANGE equations are obtained; over the surface, a boundary condition is defined. For enabling this relation, we have restricted W_{s} depending only on ϕ_A and not on $\phi_{A,\mu}$. Although we omit a direct use of this relation for generating the weak form, it serves an understanding of a boundary term and its specifications in an experimental setting.

2.1. Generating the weak form

Consider a material system composed of a three-dimensional continuum body in a reference frame, $\mathcal{B}_0 \subset \mathbb{R}^3$, with its closure, $\partial \mathcal{B}_0$, such that $\bar{\mathcal{B}} = \mathcal{B}_0 \cup \partial \mathcal{B}_0$. Material particles of the continuum body are denoted by their positions, $\boldsymbol{X}$, in the reference frame. The reference frame is an inertial frame and we choose it as fixed. In the beginning of the simulation, where the continuum body is undeformed, we set the *initial* frame as the reference frame and indicate this choice with the use of an index "0." Material particles' positions are expressed in a Cartesian coordinate system, $X_i \in \bar{\mathcal{B}}$ with $i = 1, 2, 3$, in the initial frame and they form an infinitesimal volume element $\mathrm{d}V = \mathrm{d}X_1 \, \mathrm{d}X_2 \, \mathrm{d}X_3$ as well as an infinitesimal surface element $\mathrm{d}A$. For this configuration the space is four-dimensional, $x_\mu = (t, X_i)$, with time $t \in \tau = [t_0, t_1]$ and physical space X_i such that the integral form in Eq. (10) reads

$$\int_{\tau} \int_{\mathcal{B}_0} \left(\frac{\partial \mathcal{L}}{\partial \phi_A} \delta \phi_A + \frac{\partial \mathcal{L}}{\partial \dot{\phi}_A} \delta \dot{\phi}_A + \frac{\partial \mathcal{L}}{\partial \phi_{A,i}} \delta \phi_{A,i} \right) \mathrm{d}t \, \mathrm{d}V + \int_{\tau} \int_{\partial \mathcal{B}_0} \frac{\partial W_{\mathrm{s}}}{\partial \phi_A} \delta \phi_A \, \mathrm{d}t \, \mathrm{d}A = 0 \ , \tag{11}$$

where $(\cdot)^{\cdot}$ denotes a partial time derivative since the reference frame is fixed. The integral form is continuous. In a computational environment we will solve it for discrete time steps in discrete elements (subsets of the physical space). First, we *discretize* in time. For the sake of a simplified notation (and programming) we choose constant time steps such that the time becomes the following list:

$$t = \{0, \Delta t, 2\Delta t, 3\Delta t, \ldots, t_{\mathrm{end}}\} \tag{12}$$

As a consequence, the discrete (in time) representation of ϕ_A is a list,

$$\phi_A = \{\phi_A(X_i, t = 0), \phi_A(X_i, t = \Delta t), \phi_A(X_i, t = 2\Delta t), \ldots, \phi_A(X_i, t = t_{\mathrm{end}})\} \ . \tag{13}$$

The time rate of the primitive variables read

$$\dot{\phi}_A = \frac{\partial \phi_A}{\partial t} = \frac{\phi_A - \phi_A^0}{\Delta t} \ , \tag{14}$$

where ϕ_A denotes the unknown value to be computed and ϕ_A indicates the already computed value from the last time step. This formulation converges to the analytic time rate for $\Delta t \to 0$. Since the test functions $\delta \phi_A$ are arbitrary, we may set them as constants in the beginning of a simulation. For doing so we have to eliminate $\delta \dot{\phi}_A$ from the integral form by integrating by parts

$$\int_{\tau} \int_{\mathcal{B}_0} \left(\frac{\partial \mathcal{L}}{\partial \phi_A} \delta \phi_A - \left(\frac{\partial \mathcal{L}}{\partial \dot{\phi}_A} \right)^{\cdot} \delta \phi_A + \frac{\partial \mathcal{L}}{\partial \phi_{A,i}} \delta \phi_{A,i} \right) \mathrm{d}V \, \mathrm{d}t + \int_{\mathcal{B}_0} \frac{\partial \mathcal{L}}{\partial \dot{\phi}_A} \delta \phi_A \, \mathrm{d}V \Big|_{\tau} + \int_{\tau} \int_{\partial \mathcal{B}_0} \frac{\partial W_{\mathrm{s}}}{\partial \phi_A} \delta \phi_A \, \mathrm{d}t \, \mathrm{d}A = 0 \ . \tag{15}$$

By given values of ϕ_A at two subsequent time instants like t_0 and t_1, we set the test functions zero on $\tau = [t_0, t_1]$ and obtain for every other time instant

$$\int_{\mathcal{B}_0} \left(\frac{\partial \mathcal{L}}{\partial \phi_A} \delta \phi_A - \left(\frac{\partial \mathcal{L}}{\partial \dot{\phi}_A} \right)^{\cdot} \delta \phi_A + \frac{\partial \mathcal{L}}{\partial \phi_{A,i}} \delta \phi_{A,i} \right) \mathrm{d}V + \int_{\partial \mathcal{B}_0} \frac{\partial W_{\mathrm{s}}}{\partial \phi_A} \delta \phi_A \, \mathrm{d}A = 0 \ . \tag{16}$$

Second, we discretize the physical space. The primitive variables as well as the test functions are defined on a HILBERT space with continuity k in a discrete element, E, with the DIRICHLET boundary condition on ∂E_{D},

$$\hat{\mathcal{V}} = \left\{ \phi_A, \delta \phi_A \in [\mathcal{H}^k(E)]^3 : \phi_A = \mathrm{given}, \delta \phi_A = 0 \text{ on } \partial E_{\mathrm{D}} \right\} \ . \tag{17}$$

It is technically a SOBOLEV space where also the differentiability within the domain is ensured. The continuity k shall be as high as necessary. It depends on the chosen LAGRANGEan density, which has a derivation in $\phi_{A,i}$. In the EULER–LAGRANGE equations one more integration by parts is used to "switch" the derivative in the test function to that term. Hence the regularity condition is stronger than the latter form. Therefore, the latter is called a *weak* form to be fulfilled in each element, E, finite in size. The totality of all finite elements reads the following weak form:

$$\text{Form} = \sum_{n=1}^{\text{nr of ele.}} \int_{E^n} \left(\frac{\partial \mathcal{L}}{\partial \phi_A} \delta \phi_A - \left(\frac{\partial \mathcal{L}}{\partial \dot{\phi}_A} \right)^{\cdot} \delta \phi_A + \frac{\partial \mathcal{L}}{\partial \phi_{A,i}} \delta \phi_{A,i} \right) \mathrm{d}V + \int_{\partial \mathcal{B}_0} \frac{\partial W_{\text{s}}}{\partial \phi_A} \delta \phi_A \, \mathrm{d}A \ . \tag{18}$$

The external work done on the surface is given, $W_{\text{s}} = W_{\text{s}}(t, X_i, \phi_A)$, and the surface element $\mathrm{d}A$ denotes an integration over the surface belonging to boundary $\partial \mathcal{B}_0$ excluding DIRICHLET boundaries. On the DIRICHLET boundaries the numerical value of ϕ_A is given, since we know them $\delta \phi_A$ on the DIRICHLET boundaries vanishes, called GALERKIN approach. The weak form is a general integral form applicable to all reversible systems defined by a LAGRANGEan depending on primitive variables and their derivatives.

2.2. Elasticity theory

In elasticity the primitive variable is the displacement:

$$\phi_A = u_i \ , \quad u_i = x_i - X_i \ , \tag{19}$$

where the displacement is the deviation from the reference (initial) position, X_i, to the current position, x_i. The LAGRANGEan density for the elasticity reads

$$\mathcal{L} = \frac{1}{2} \rho_0 \dot{u}_i \dot{u}_i - w + \rho_0 f_i u_i \ , \tag{20}$$

where the first term denotes the *kinetic* energy, the second term indicates the *stored* or deformation energy, and the third term is called the *potential* energy. In the case of elasticity, the stored energy density (energy per volume) w depends on displacement and its first derivative in space. Its exact form relies on the underlying material. The conservative force f_i is simply the gravitational specific force (force per mass). We present two different material models in the following sections, they only differ in the definition of the stored energy density, w. On NEUMANN boundaries the energy expression

$$W_{\text{s}} = \hat{t}_i u_i \tag{21}$$

implements a traction vector $\hat{t}_i$ in the unit of stress, modeling a mechanical loading on a part of the surface. By inserting the latter in Eq. (18) we obtain the weak form discrete in time and space,

$$\text{Form} = \sum_{n=1}^{\text{nr of ele.}} \int_{E^n} \left(f_i \delta u_i - \rho_0 \frac{u_i - 2u_i^0 + u_i^{00}}{\Delta t \Delta t} \delta u_i - \frac{\partial w}{\partial u_{i,j}} \delta u_{i,j} \right) \mathrm{d}V + \int_{\partial \mathcal{B}_0} \hat{t}_i \delta u_i \, \mathrm{d}A \ . \tag{22}$$

This weak form can be solved by using $k = 1$ since we have only first order derivative in u_i. In other words, linear continuous standard elements will be used. Indeed the latter weak form can be solved for various definitions of the stored energy density. It is of importance to note that the term:

$$\frac{\partial w}{\partial u_{i,j}} \ , \tag{23}$$

is called PIOLA stress:

$$P_{ji} = \frac{\partial w}{\partial F_{ij}} \ , \tag{24}$$

since the deformation gradient, F_{ji}, leads to

$$F_{ji} = \frac{\partial x_j}{\partial X_i} = \delta_{ji} + u_{j,i} \ , \quad \frac{\partial w}{\partial u_{i,j}} = \frac{\partial w}{\partial F_{kl}} \frac{\partial F_{kl}}{\partial u_{i,j}} = P_{lk} \frac{\partial u_{k,l}}{\partial u_{i,j}} = P_{lk} \delta_{ki} \delta_{lj} = P_{ji} \ . \tag{25}$$

The polynomial degree of Eq. (23) states the degree of the material model. The stored energy density is one degree higher, for example, for a linear material model w is quadratic. By defining the LAGRANGEan density in Eq. (20), we have introduced several assumptions. First, we have assumed that it be independent of time. In

other words, f_i is a conservative force and does not depend on time explicitly. Second, we assume that the kinetic energy depends on $u_i^{\cdot}$ and the stored energy depends on u_i and $u_{i,j}$. In other words, we exclude viscoelasticity by neglecting a dependence on $u_{i,j}^{\cdot}$. Third, we use the deformation gradient or the GREEN–LAGRANGE strain measure

$$E_{ij} = \frac{1}{2}u_{k,i}u_{k,j} + u_{(i,j)} \ , \tag{26}$$

instead of displacement dependence in the stored energy. So the stored energy is

$$w = \tilde{w}(X_i, F_{ij}) = \bar{w}(X_i, E_{ij}) \ . \tag{27}$$

As a special case, for homogeneous materials the dependency on X_i vanishes. Due to the principle of objectivity, the scalar function depends on the invariants of the deformation gradient or strain.

3. Variational formulation for the second order theory

In order to generalize the proposed method, we redefine the LAGRANGEan density as including the second derivatives of the primitive variables

$$\mathcal{L} = \mathcal{L}(x_\mu, \phi_A, \phi_{A,\mu}, \phi_{A,\mu\nu}) \ , \quad \phi_{A,\mu} = \frac{\partial \phi_A}{\partial x_\mu} \ , \quad \phi_{A,\mu\nu} = \frac{\partial^2 \phi_A}{\partial x_\mu \partial x_\nu} \ . \tag{28}$$

In this configuration the state space reads

$$\{\phi_A, \phi_{A,\mu}, \phi_{A,\mu\nu}\} \tag{29}$$

with the following variations:

$$\phi'_A = \phi_A + \varepsilon\delta\phi_A \ , \quad \phi'_{A,\mu} = \phi_{A,\mu} + \varepsilon\delta\phi_{A,\mu} \ , \quad \phi'_{A,\mu\nu} = \phi_{A,\mu\nu} + \varepsilon\delta\phi_{A,\mu\nu} \ . \tag{30}$$

The same action definition and the variation of it leads to

$$\mathcal{L}' = \mathcal{L} + \frac{\partial \mathcal{L}}{\partial \phi_A}\varepsilon\delta\phi_A + \frac{\partial \mathcal{L}}{\partial \phi_{A,\mu}}\varepsilon\delta\phi_{A,\mu} + \frac{\partial \mathcal{L}}{\partial \phi_{A,\mu\nu}}\varepsilon\delta\phi_{A,\mu\nu} \ , \tag{31}$$

and provides the following integral form:

$$\int_\Omega \left(\frac{\partial \mathcal{L}}{\partial \phi_A}\delta\phi_A + \frac{\partial \mathcal{L}}{\partial \phi_{A,\mu}}\delta\phi_{A,\mu} + \frac{\partial \mathcal{L}}{\partial \phi_{A,\mu\nu}}\delta\phi_{A,\mu\nu} \right) \mathrm{d}\Sigma +$$
$$+ \int_{\partial\Omega} \frac{\partial W_{\mathrm{s}}}{\partial \phi_A}\delta\phi_A \, \mathrm{d}\Gamma + \int_{\partial\Omega} \frac{\partial W_{\mathrm{s}}}{\partial \phi_{A,\mu}}\delta\phi_{A,\mu} \, \mathrm{d}\Gamma + \int_{\partial\partial\Omega} \frac{\partial W_{\mathrm{e}}}{\partial \phi_A}\delta\phi_A \, \mathrm{d}\Pi + \int_{\partial\partial\Omega} \frac{\partial W_{\mathrm{e}}}{\partial \phi_{A,\mu}}\delta\phi_{A,\mu} \, \mathrm{d}\Pi = 0 \ , \tag{32}$$

after using the principle of least action and dividing by ε. By using the same justification as in the last section, we allow W_{s} on surface $\mathrm{d}\Gamma$ and W_{e} on edge $\mathrm{d}\Pi$ depend only on ϕ_A and $\phi_{A,\mu}$ but not on $\phi_{A,\mu\nu}$.

3.1. Generating the weak form

As in the last section, again for $x_\mu = (t, X_i)$ with $t \in \tau = [t_0, t_1]$ and $X_i \in \mathcal{B}_0$, we obtain

$$\int_\tau \int_{\mathcal{B}_0} \left(\frac{\partial \mathcal{L}}{\partial \phi_A}\delta\phi_A + \frac{\partial \mathcal{L}}{\partial \phi_A^{\cdot}}\delta\phi_A^{\cdot} + \frac{\partial \mathcal{L}}{\partial \phi_{A,i}}\delta\phi_{A,i} + \frac{\partial \mathcal{L}}{\partial \phi_A^{\cdot\cdot}}\delta\phi_A^{\cdot\cdot} + \frac{\partial \mathcal{L}}{\partial \phi_{A,i}^{\cdot}}\delta\phi_{A,i}^{\cdot} + \frac{\partial \mathcal{L}}{\partial \phi_{A,ij}}\delta\phi_{A,ij} \right) \mathrm{d}V \, \mathrm{d}t +$$
$$+ \int_\tau \int_{\partial\mathcal{B}_0} \frac{\partial W_{\mathrm{s}}}{\partial \phi_A}\delta\phi_A \, \mathrm{d}t \, \mathrm{d}A + \int_\tau \int_{\partial\mathcal{B}_0} \left(\frac{\partial W_{\mathrm{s}}}{\partial \phi_A^{\cdot}}\delta\phi_A^{\cdot} + \frac{\partial W_{\mathrm{s}}}{\partial \phi_{A,i}}\delta\phi_{A,i} \right) \mathrm{d}t \, \mathrm{d}A +$$
$$+ \int_\tau \int_{\partial\partial\mathcal{B}_0} \frac{\partial W_{\mathrm{e}}}{\partial \phi_A}\delta\phi_A \, \mathrm{d}t \, \mathrm{d}\ell + \int_\tau \int_{\partial\partial\mathcal{B}_0} \left(\frac{\partial W_{\mathrm{e}}}{\partial \phi_A^{\cdot}}\delta\phi_A^{\cdot} + \frac{\partial W_{\mathrm{e}}}{\partial \phi_{A,i}}\delta\phi_{A,i} \right) \mathrm{d}t \, \mathrm{d}\ell = 0 \ . \tag{33}$$

In the time discrete fashion we eliminate terms with rates of test functions by integrating by parts. Then we use the fact that the values ϕ_A^0 and ϕ_A^{00} are known in the beginning such that $\delta\phi_A$ vanishes. After discretization in space, we obtain the following weak form

$$\mathrm{Form} = \sum_{n=1}^{\mathrm{nr\ of\ ele.}} \int_{E^n} \left(\frac{\partial \mathcal{L}}{\partial \phi_A}\delta\phi_A - \left(\frac{\partial \mathcal{L}}{\partial \phi_A^{\cdot}}\right)^{\cdot}\delta\phi_A + \frac{\partial \mathcal{L}}{\partial \phi_{A,i}}\delta\phi_{A,i} + \left(\frac{\partial \mathcal{L}}{\partial \phi_A^{\cdot\cdot}}\right)^{\cdot\cdot}\delta\phi_A - \left(\frac{\partial \mathcal{L}}{\partial \phi_{A,i}^{\cdot}}\right)^{\cdot}\delta\phi_{A,i} + \frac{\partial \mathcal{L}}{\partial \phi_{A,ij}}\delta\phi_{A,ij} \right) \mathrm{d}V +$$
$$+ \int_{\partial\mathcal{B}_0} \left(\left(\frac{\partial W_{\mathrm{s}}}{\partial \phi_A} - \left(\frac{\partial W_{\mathrm{s}}}{\partial \phi_A^{\cdot}}\right)^{\cdot}\right)\delta\phi_A + \frac{\partial W_{\mathrm{s}}}{\partial \phi_{A,i}}\delta\phi_{A,i} \right) \mathrm{d}A + \int_{\partial\partial\mathcal{B}_0} \left(\left(\frac{\partial W_{\mathrm{e}}}{\partial \phi_A} - \left(\frac{\partial W_{\mathrm{e}}}{\partial \phi_A^{\cdot}}\right)^{\cdot}\right)\delta\phi_A + \frac{\partial W_{\mathrm{e}}}{\partial \phi_{A,i}}\delta\phi_{A,i} \right) \mathrm{d}\ell \ . \tag{34}$$

The extension to the second order theory introduced many different boundary conditions. All of them have to be given and they are discussed by many researchers. Mainly we have boundary terms acting on surface and additionally terms acting on edges. Since now not only ϕ_A but also its derivative is involved, we need to approximate the discrete representation of ϕ_A from a SOBOLEV space,

$$\hat{\mathcal{V}} = \left\{ \phi_A, \delta\phi_A \in [\mathcal{H}^k(E)]^3 : \phi_A = \text{given}, \delta\phi_A = 0 \text{ on } \partial E_\mathrm{D} \right\} , \tag{35}$$

with $k \geq 2$.

3.2. Strain gradient elasticity theory

In strain gradient elasticity the primitive variable is the displacement:

$$\phi_A = u_i . \tag{36}$$

For being able to compare the elasticity and strain gradient elasticity we implement exactly the same surface energy and neglect the edge energy,

$$W_\mathrm{s} = \hat{t}_i u_i , \quad W_\mathrm{e} = 0 , \tag{37}$$

where the traction vector $\hat{t}_i$ denotes again the mechanical load on the NEUMANN boundary. These boundary conditions are heavily discussed in the literature and their application to experimental mechanics is very challenging. For some useful interpretations of these surface and edge energies and how they affect the solution, among others, we refer to Auffray et al. (2015), Javili et al. (2013), Steigmann and dell'Isola (2015). Although we obtained these additional terms on boundaries, they are challenging to justify. For the specific case of a quadratic energy, by using variational formulation in Mindlin (1965), by using principle of virtual power in Polizzotto (2013a), it is shown that W_s and W_e may include relations leading to a dependency in u_i and $u_{i,j}$. Moreover, the aforementioned relations can be rewritten, see Polizzotto (2013a, Sect. 5), in order to relate them to measurable quantities like surface tension (energy). Such an analysis results in W_s depending on u_i and surface normal component of gradient of displacement. Herein we have even proposed to involve dependencies on $\dot{u}_i$. Unfortunately, we lack a clear justification of experimental feasibility for such dependencies. For simplicity we choose Eq. (37) to implement such that a comparison with the well-known linear elasticity is possible.

For non-polar materials we propose the following LAGRANGEan density:

$$\mathcal{L} = \frac{1}{2}\rho_0 \dot{u}_i \dot{u}_i - w + \rho_0(f_i u_i + l_{ij} u_{j,i}) . \tag{38}$$

The first term is an inertial term. Herein we simplify the formulation by assuming that only the velocity and ordinary momentum (mass times velocity) takes part in this term, see Polizzotto (2013a), Polizzotto (2013b) for an elaborate discussion. So the inertial term consists of the kinetic energy due to the macroscopic velocity for non-polar materials. For a polar material this term would have a term with spin, too. The second term is again the stored energy; however, the list of argumentation is amended such that the stored energy depends not only on the first but also on the second gradient of the primitive variable, i.e., displacement,

$$w = w(X_i, E_{ij}, E_{ij,k}) . \tag{39}$$

We will restrict the formulation to homogeneous materials such that the dependency on material particles' positions, X_i, vanishes. The third term denotes the energy due to the volumetric effects. The first part, $f_i u_i$, is the specific energy because of the gravitational forces creating a translational displacement (implied by the linear momentum). The second part, $l_{ij} u_{j,i}$, is the specific volumetric energy leading to a rotational displacement (implied by the angular momentum). For a non-polar medium this term vanishes. By inserting the LAGRANGEan density we obtain the weak form for a non-polar material with traction type boundaries:

$$\text{Form} = \sum_{n=1}^{\text{nr of ele.}} \int_{E^n} \left(\rho_0 f_i \delta u_i - \rho_0 \frac{u_i - 2u_i^0 + u_i^{00}}{\Delta t \Delta t} \delta u_i - \frac{\partial w}{\partial u_{i,j}} \delta u_{i,j} + \rho_0 l_{ji} \delta u_{i,j} - \right.$$
$$\left. -\frac{1}{\Delta t \Delta t} \left(\frac{\partial w}{\partial u_{i,j}} - 2\frac{\partial w^0}{\partial u_{i,j}^0} + \frac{\partial w^{00}}{\partial u_{i,j}^{00}} \right) \delta u_{i,j} - \frac{\partial w}{\partial u_{i,jk}} \delta u_{i,jk} \right) \mathrm{d}V + \int_{\partial \mathcal{B}_0} \hat{t}_i \delta u_i \, \mathrm{d}A , \tag{40}$$

where the following notation is introduced

$$w^0 = w(E_{ij}^0, E_{ij,k}^0) , \quad w^{00} = w(E_{ij}^{00}, E_{ij,k}^{00}) ,$$
$$E_{ij}^0 = \frac{1}{2} u_{k,i}^0 u_{k,j}^0 + u_{(i,j)}^0 , \quad E_{ij}^{00} = \frac{1}{2} u_{k,i}^{00} u_{k,j}^{00} + u_{(i,j)}^{00} , \tag{41}$$

with the GREEN–LAGRANGE strain tensor, E_{ij}, and its values in the last and second last time steps, E_{ij}^0, E_{ij}^{00}, respectively. The latter form can be solved by using $k = 2$ since we have second order derivative in u_i. In other words, we will use quadratic continuous standard elements.

4. Applications

The weak forms in Eq. (22) for elasticity and in Eq. (40) for strain gradient elasticity are general forms applicable to linear as well as nonlinear materials. Moreover, since we use a nonlinear strain measure, namely the GREEN–LAGRANGE strain tensor, the formulation captures geometric nonlinearities as well. Other then elastic response, we have not made any assumptions so far. In this section we will present a computational tool for solving the presented nonlinear weak forms numerically. By using the Python programming language, see Oliphant (2007), we develop a code for obtaining solution of weak forms by exploiting the collection of open-source packages developed under the FEniCS project, see Hoffman et al. (2005), Logg et al. (2011), Jones et al. (2001). We use finite element method in space and finite difference method in time. For the visualization of results we use ParaView, see Ahrens et al. (2011), Ayachit (2015).

Three examples are shown for linear elastic, hyperelastic, and linear strain gradient elastic materials. All examples have nonlinear weak forms such that the weak form needs to be linearized before solving. This linearization is gained by a symbolic derivation of the weak form, before assembly. Therefore, the linearization is at the level of the partial differential equations. The derivation is fully automatized by using symbolic derivative functionality, see Alnæs and Mardal (2010), Alnaes and Mardal (2012). Moreover, we have implemented the code by defining the stored energy function. Its derivation, precisely the solution of Eq. (23), is computed by using the aforementioned symbolic derivative functionality. This abstraction is of paramount importance, the following three examples differ only in the definition of the stored energy function.

For learning the basics of programming in Python for FEniCS ecosystem, see Langanten and Logg (2017). For several engineering applications by using FEniCS, see Abali (2017a). In order to encourage further research, we publish all used codes in Abali (2017b) under the GNU Public license as stated in Gnu Public (2007).

4.1. Example for linear elasticity

A structure made of an engineering steel can be modeled with a linear elastic material if the mechanical loading generates stresses less than the yield stress such that no plastic deformation occurs. Consider a thin plate modeled as a three-dimensional structure under a mechanical loading. Under a concentrated loading, plate underlies a large deformation (with respect to the geometric dimensions). For the linear model of a homogeneous steel, the generic form of the quadratic scalar function reads

$$w = E_{ij} C_{ijkl} E_{kl} \ , \tag{42}$$

where C_{ijkl} is called the *stiffness* or *elasticity* tensor with 21 independent coefficients since

$$C_{ijkl} = C_{jikl} \ , \quad C_{ijkl} = C_{ijlk} \ , \quad C_{ijkl} = C_{klij} \ , \tag{43}$$

effected by the symmetric strain, $E_{ij} = E_{ji}$. This case is applicable for any material class. Existing crystal symmetries decreases the number of independent coefficients. For example, in the case of an isotropic material, the representation of this rank four tensor simplifies to

$$C_{ijkl} = \lambda \delta_{ij} \delta_{kl} + \mu_1 \delta_{ik} \delta_{jl} + \mu_2 \delta_{il} \delta_{jk} \ , \tag{44}$$

see for example Abali et al. (2015, Appendix) for a derivation. By inserting the stiffness tensor into the energy density we obtain the so-called ST. VENANT–KIRCHHOFF model for the stored energy:

$$w = \lambda \frac{1}{2} E_{ii} E_{jj} + \mu E_{ij} E_{ji} \ , \tag{45}$$

where $\mu = \mu_1 = \mu_2$ since strain is symmetric and the so-called LAME parameters, λ, μ, are given by YOUNG's modulus, E, and POISSON's ratio, ν as follows

$$\lambda = \frac{E\nu}{(1+\nu)(1-2\nu)} \ , \quad \mu = \frac{E}{2(1+\nu)} \ . \tag{46}$$

The strain measure is nonlinear, thus, the geometric nonlinearities are computed accurately. The stored energy density is quadratic in strain, therefore, the material model in Eq. (23) is linear. We simulate a plate of an AISI steel with the following parameters:

$$\rho_0 = 8.1 \cdot 10^{-9} \,\mathrm{Mg/mm}^3 \,, \quad E = 200 \cdot 10^3 \,\mathrm{MPa} \,, \quad \nu = 0.3 \,. \tag{47}$$

The plate is of $1000 \times 600 \times 20 \,\mathrm{mm}$ and its surface lies in $X_1 X_2$-plane. The concentrated force is modeled by a GAUSSian distribution, increasing linearly in time

$$\tilde{t} = at \exp \left(b(X_1 - \bar{X}_1)^2 + b(X_2 - \bar{X}_2)^2 \right) \,, \tag{48}$$

such that $\hat{t}_i = -\tilde{t} N_i$ applies on a small area on top of the plate against the plane normal, N_i. The force increases linearly in time. The gravitational forces are implemented, $f_i = (0, 0, -9850) \,\mathrm{N/Mg}$, although the deformation due to them is negligible (small with respect to the deformation caused by the loading). The transient solution of the weak form in Eq. (22) provides the displacement field, $u(t, X_i)$, as expected, for the convergence see App. A. The response is immediate and the deformation goes back to the initial value after unloading. For example, the deformation can be seen in Fig. 1 at the time instant of maximum force applied on the top of the plate.
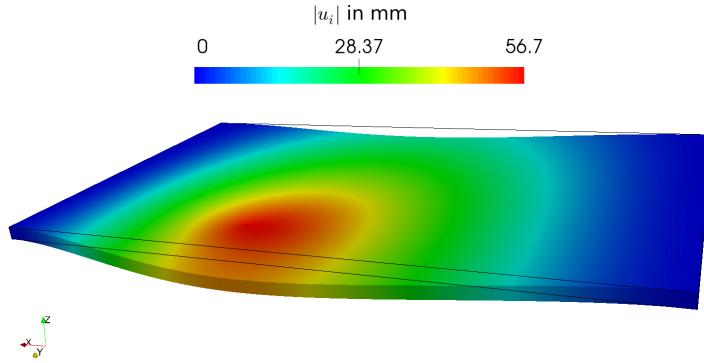

Figure 1: Deformation of the three-dimensional elastic plate, shown without scaling, colors denote the magnitude of the displacement field, $|u_i|$.

4.2. Example for nonlinear elasticity

A soft material, for example a silicon gel, has a more localized strain distribution leading to sharp strain alterations in the structure. A nonlinear material model is necessary to capture this effect. For a silicon gel we implement the neo-HOOKEan energy density:

$$w = \lambda \frac{1}{2} \ln^2(\det(\boldsymbol{F})) + \mu \left(\frac{F_{ji} F_{ji}}{2} - \frac{\delta_{jj}}{2} - \ln(\det(\boldsymbol{F})) \right) \,, \tag{49}$$

where the deformation gradient occurs in a highly nonlinear fashion such that its derivative, the stress tensor, is nonlinear, too. The material parameters for the silicon gel TSE3062 are as follows

$$\rho_0 = 1.1 \cdot 10^{-9} \,\mathrm{Mg/mm}^3 \,, \quad \nu = 0.4 \,, \quad E = 89 \,\mathrm{MPa} \,. \tag{50}$$

Since taking derivative of the energy is handled automatically, the implementation is the same as in the previous example, only the stored energy definition changes. We solve the silicon gel filled in a cup under a line loading by using the following GAUSSian distribution:

$$\tilde{t} = at \exp \left(b(X_2 - \bar{X}_2)^2 \right) \,. \tag{51}$$

Since the deformation in a soft matter is much greater than the gravitational based deflection, we assume $f_i = 0$. The computation is as expected, for the convergence see App. B. The deformation at the time when the force reaches its maximum value can be seen in Fig. 2.
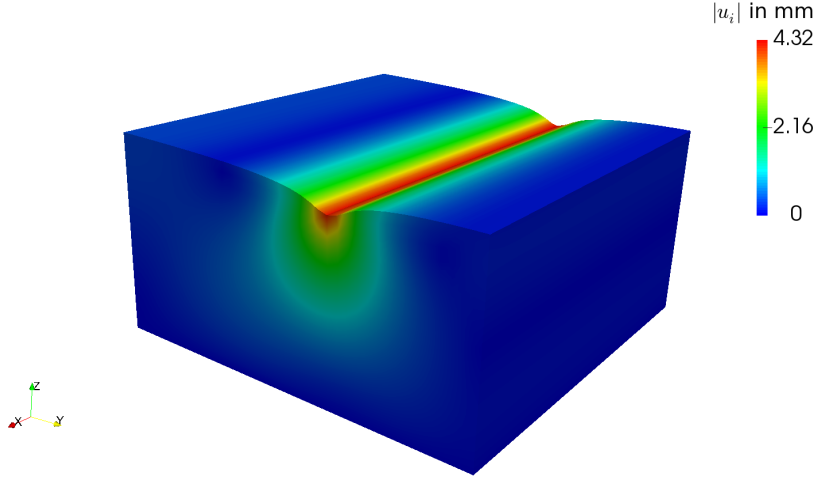
Figure 2: Deformation of the silicon gel filled in a box of $80 \times 80 \times 40\,\mathrm{mm}$, presented without any scaling, colors denote the magnitude of the displacement field, $|u_i|$.

4.3. Example for linear strain gradient elasticity

In order to generalize the stored energy formulation, we start with a generic representation for linear homogeneous materials:

$$w = w(E_{ij}, E_{ij,k}) = E_{ij}C_{ijkl}E_{kl} + E_{ij,k}D_{ijklmn}E_{lm,n} + E_{ij}G_{ijklm}E_{kl,m} \ . \tag{52}$$

For isotropic materials the mixed term, G_{ijklm}, vanishes, see dell'Isola et al. (2009). For an isotropic linear material we obtain

$$\begin{aligned}
C_{ijkl} &= \bar{c}_{01}\delta_{ij}\delta_{kl} + \bar{c}_{02}\delta_{ik}\delta_{jl} + \bar{c}_{03}\delta_{il}\delta_{jk} \ , \\
D_{ijklmn} &= c_{01}\delta_{ij}\delta_{kl}\delta_{mn} + c_{02}\delta_{ij}\delta_{km}\delta_{ln} + c_{03}\delta_{ij}\delta_{kn}\delta_{ml} + c_{04}\delta_{ik}\delta_{jl}\delta_{mn} + \\
&\quad + c_{05}\delta_{ik}\delta_{jm}\delta_{ln} + c_{06}\delta_{ik}\delta_{jn}\delta_{lm} + c_{07}\delta_{il}\delta_{jk}\delta_{mn} + c_{08}\delta_{il}\delta_{jm}\delta_{kn} + \\
&\quad + c_{09}\delta_{il}\delta_{jn}\delta_{mk} + c_{10}\delta_{im}\delta_{jk}\delta_{ln} + c_{11}\delta_{im}\delta_{jl}\delta_{kn} + c_{12}\delta_{im}\delta_{jn}\delta_{lk} + \\
&\quad + c_{13}\delta_{in}\delta_{jk}\delta_{lm} + c_{14}\delta_{in}\delta_{jl}\delta_{km} + c_{15}\delta_{in}\delta_{jm}\delta_{kl} \ ,
\end{aligned} \tag{53}$$

see Abali et al. (2015, Appendix) for a derivation of these forms. From the quadratic energy we realize the following conditions:

$$C_{ijkl} = C_{klij} \ , \quad D_{ijklmn} = D_{lmnijk} \ . \tag{54}$$

Moreover, the symmetry in strains, $E_{ij} = E_{ji}$, implies further conditions:

$$C_{ijkl} = C_{jikl} \ , \quad C_{ijkl} = C_{ijlk} \ , \quad D_{ijklmn} = D_{jiklmn} \ , \quad D_{ijklmn} = D_{ijkmln} \ . \tag{55}$$

By applying all of these conditions we obtain

$$\begin{aligned}
C_{ijkl} &= c_1\delta_{ij}\delta_{kl} + c_2(\delta_{ik}\delta_{jl} + \delta_{il}\delta_{jk}) \ , \\
D_{ijklmn} &= c_3(\delta_{ij}\delta_{kl}\delta_{mn} + \delta_{in}\delta_{jk}\delta_{lm} + \delta_{ij}\delta_{km}\delta_{ln} + \delta_{ik}\delta_{jn}\delta_{lm}) + c_4\delta_{ij}\delta_{kn}\delta_{ml} + \\
&\quad + c_5(\delta_{ik}\delta_{jl}\delta_{mn} + \delta_{im}\delta_{jk}\delta_{ln} + \delta_{ik}\delta_{jm}\delta_{ln} + \delta_{il}\delta_{jk}\delta_{mn}) + c_6(\delta_{il}\delta_{jm}\delta_{kn} + \delta_{im}\delta_{jl}\delta_{kn}) + \\
&\quad + c_7(\delta_{il}\delta_{jn}\delta_{mk} + \delta_{im}\delta_{jn}\delta_{lk} + \delta_{in}\delta_{jl}\delta_{km} + \delta_{in}\delta_{jm}\delta_{kl}) \ .
\end{aligned} \tag{56}$$

Hence, for an isotropic linear homogeneous material including strain gradients (of order one), the generic energy formulation consists of seven material parameters.

The five newly introduced parameters, viz., c_3, c_4, c_5, c_6, c_7, change the deformation of the structure. We have been able to detect one parameter, c_6, imposing the so-called size effect in a beam bending. In order to demonstrate how the proposed material model simulates the size-effect in a beam bending, we construct a beam of length ℓ. It is a slender beam, $\ell \times \ell/30 \times \ell/30$, out of aluminum with the following properties:

$$\rho_0 = 2.7 \cdot 10^{-9}\,\mathrm{Mg/mm}^3 \ , \quad \nu = 0.33 \ , \quad E = 72 \cdot 10^3\,\mathrm{MPa} \ , \tag{57}$$

$$c_1 = \lambda = \frac{E\nu}{(1+\nu)(1-2\nu)} \ , \quad c_2 = \mu = \frac{E}{2(1+\nu)} \ .$$
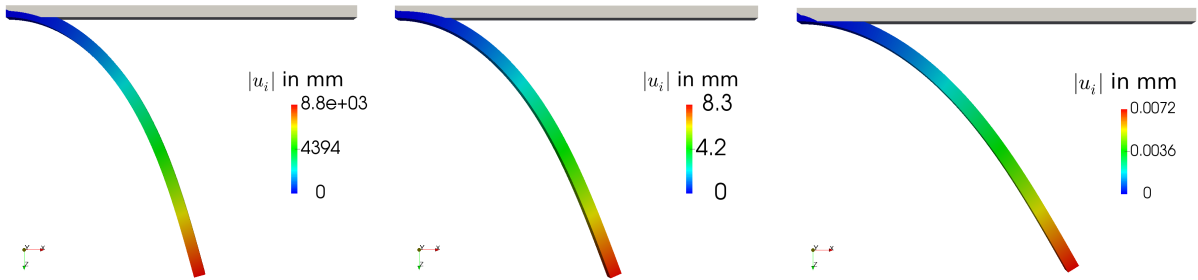
Figure 3: Deformation of the three-dimensional cantilever beam bending with $c_6 = 1000\,\mathrm{N}$, without any scaling, colors denote the magnitude of the displacement field, $|u_i|$. Left: 10 m beam. Middle: 10 mm beam. Right: 10 μm beam.

By clamping one end at $x = 0$ and shearing the other end at $x = \ell$, we simulate transiently the displacement in three-dimensional beam structure for various parameters. The solution is as expected, for the convergence see App. C. The shear force is applied on the whole cross section at $x = \ell$ and it increases linearly in 1 s up to 10 N for a beam of length $\ell = 100\,\mathrm{mm}$. We set $c_3 = c_4 = c_5 = c_7 = 0$ and vary c_6 parameter. In Table 1 the role of c_6 can be studied. We recall that for a 100 mm long beam such displacements are considered as large deformations.

Table 1: Maximum deflection.

c_6 in N	$u_i^{\mathrm{max.}}$ in mm
0	4.21286
1	4.21285
10	4.21274
100	4.21164
1000	4.20077
10 000	4.10762

We refrain ourselves from verifying the results to any analytic solution applicable to geometrically linear cases. The parameter c_6 causes a stiffness in the shear bending. By setting $c_6 = 0$ we obtain the results for elasticity. Interestingly, according to the introduction of the length-scale $\sqrt{c_6/E}$, see for a discussion of the length-scale in Giorgio (2016), this particular effect depends on the size of the beam. In order to present this feature, we simulate the same beam of $\ell \times \ell/30 \times \ell/30$ in three different lengths: $\ell = 10\,\mathrm{m}$, $\ell = 10\,\mathrm{mm}$, and $\ell = 10\,\mathrm{μm}$. All material parameters are identical for these simulations with $c_6 = 1000\,\mathrm{N}$. Since the lengths are different, the deformation is different quantitatively. In order to obtain the same amount of deformation per length, we can match the shearing force by applying the same force per beam length square. This ratio should be held constant. As a reasoning consider the limiting case, where the force is so small that there occurs a geometrically linear deformation. The maximum deflection per beam length is proportional to

$$u_{\mathrm{max}} = \frac{F\ell^3}{3EI} \ , \quad I = \frac{\ell^4}{12 \cdot 30^4} \Rightarrow \frac{u_{\mathrm{max}}}{\ell} \propto \frac{F}{\ell^2} \ . \tag{58}$$

By choosing a large F value and holding its ratio per beam length square fixed, we observe in Fig. 3 that the qualitative deformation changes depending on the beam length, shorter beams present more stiffening. This stiffening effect is observed in experiments exactly as simulated herein. Often, this phenomenon is called size-effect indicating that the deformation behavior changes depending on the size of the structure. Exactly this phenomenon is a possible procedure of determining the newly introduced c_6 parameter. A measurement of the tip deflection of beams in different length-scales is compared to computations with a particular c_6 parameter. This determined c_6 parameter can be used for structures larger than $\sqrt{c_6/E}$. For example, suppose that we have a material with $c_6 = 10\,\mathrm{N}$ and $E = 72\,000\,\mathrm{MPa}$, in this case $\sqrt{c_6/E} = 11.79\,\mathrm{μm}$ can be interpreted as the upper limit of the characteristic length, in the beam bending this length is the beam length. A beam shorter than the upper limit, the substructure becomes relevant such that we have to model it in a detailed matter. In the numerical examples above, we have ignored this fact and devoted ourselves to interpreting the effect of the

newly introduced parameter.

In order to present the reason why this stiffening effect emerges, we perform different simulations for a beam of $\ell = 10\,\mu$m with $c_6 = 0$ and $c_6 = 1000\,$N. All deformations are plotted on top of each other in Fig. 4. Although
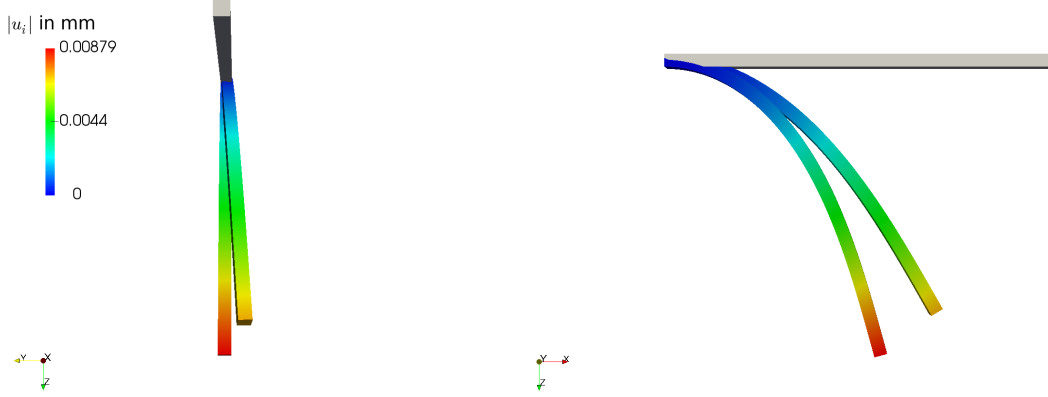

Figure 4: Deformation of the three-dimensional cantilever beam bending with $c_6 = 0$ and $c_6 = 1000\,$N, without using any scaling. Left: front view. Right: side view. Colors denote the magnitude of the displacement field, $|u_i|$, on a $10\,\mu$m length beam. The stiffening effect is due to an additional twist on the beam neutral axis such that $c_6 \neq 0$ results in a skew bending.

the shearing force is acting on the whole cross section, there is a skew bending introduced with $c_6 \neq 0$. In order to preserve the positive definiteness of the stored energy, we choose c_6 positive, see dell'Isola et al. (2009, Sect. 4). We interpret the results as if an additional rotation such as a twist is implied. Instead of a pure shear bending, there is a shear bending and a torsion on x_1-axis (positively) due to c_6 parameter bringing in the effect of the internal substructure.

5. Conclusion

We have presented a general theory of generalized elasticity by means of LAGRANGEan mechanics by using a variational formulation. This method leads naturally to a weak form, which is an important benefit of using this strategy. By obtaining the weak form, we can implement a numerical computation of any physical system. In this work, we demonstrated the variational formulation in elasticity as well as in strain gradient elasticity theory. For the sake of presenting a general approach, we have left the stored energy density undefined. In order to simulate concrete examples, we defined a stored energy density for linear and nonlinear elasticity, as well as for linear strain gradient elasticity. By using finite element method in space and finite difference method in time, we implemented and solved concrete applications.

Although formulations for generating the weak form for elasticity exist in the literature, they start by postulating the balance of the linear momentum and then defining the stress tensor. In our formulation we postulate the LAGRANGEan density and define the stored energy density. For the linear and nonlinear elasticity the same weak form is acquired in two methods. This is not the case for strain gradient elasticity, there are various approaches leading to different formulations. We believe that showing the approach over a variational formulation enriches the existing knowledge about computational mechanics and defines another path of implementing through energy, which is the direct observable in measurements. Especially in rubber-like materials, modeling the stored energy is more convenient than the stress. Moreover, by exploiting the FEniCS ecosystem, we have coded and solved the applications in the same approach as in the methodology—just defining the stored energy density. Since the presented strain gradient theory seems to be a general approach, the only difference between various second order theories relies on the definition of the stored energy density. All codes are publicly available in Abali (2017b) licensed under Gnu Public (2007) and we invite researches to test their theories with our code in order to gain an insight for strength and deficiencies, as well as applicability to the experimental outcomes.

A. Convergence for linear elasticity

Standard h-convergence has been conducted by decreasing the mesh size in every tetrahedron. We use the same geometry and boundary conditions and compute L_2 norm of the solution (displacement vector) over the whole mesh. We restrict the analysis to the first 5 time steps, t_1, t_2, t_3, t_4, t_5 and expect a linear relation for every time step between (log of) degrees of freedom (dofs) and (log of) L_2 norm. The results are compiled in Table 2 and shown in Fig. 5.

Table 2: Convergence analysis for linear elastic transient FEM computation.

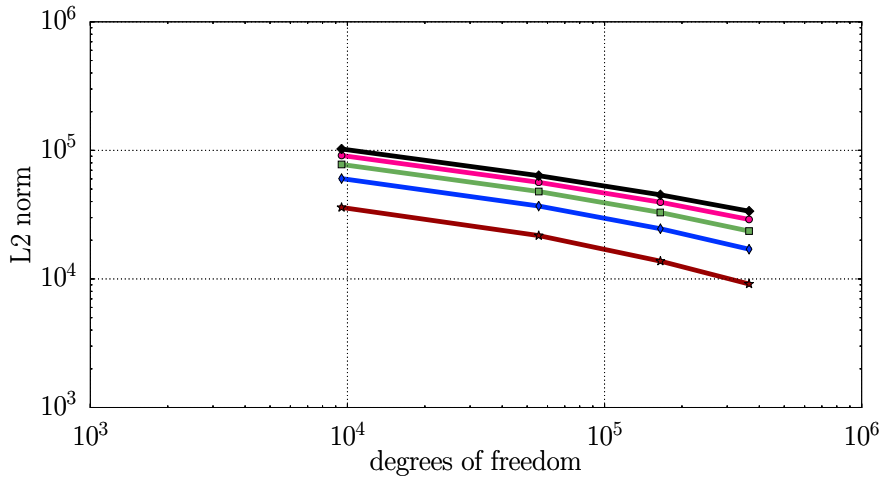|	t_1	t_2	t_3	t_4	t_5
dofs	L_2 norm				
9 486	35 977	60 346	77 717	91 282	102 519
55 449	21 739	16 907	47 856	56 441	63 564
164 892	13 755	24 574	32 871	39 524	45 089
364 815	9 135	17 040	23 577	28 023	33 666

Figure 5: For the linear elastic transient FEM, plot of degrees of freedom versus L_2 norm over the whole mesh in a log-log scale. Colors denote different time steps.

B. Convergence for nonlinear elasticity

Standard h-convergence has been conducted with the same geometry and boundary conditions for the first 5 time steps, t_1, t_2, t_3, t_4, t_5. The results are compiled in Table 3 and shown in Fig. 6.

C. Convergence for linear strain gradient elasticity

Standard h-convergence has been conducted with the same geometry and boundary conditions for the first 5 time steps, t_1, t_2, t_3, t_4, t_5. The results are compiled in Table 4 and shown in Fig. 7.
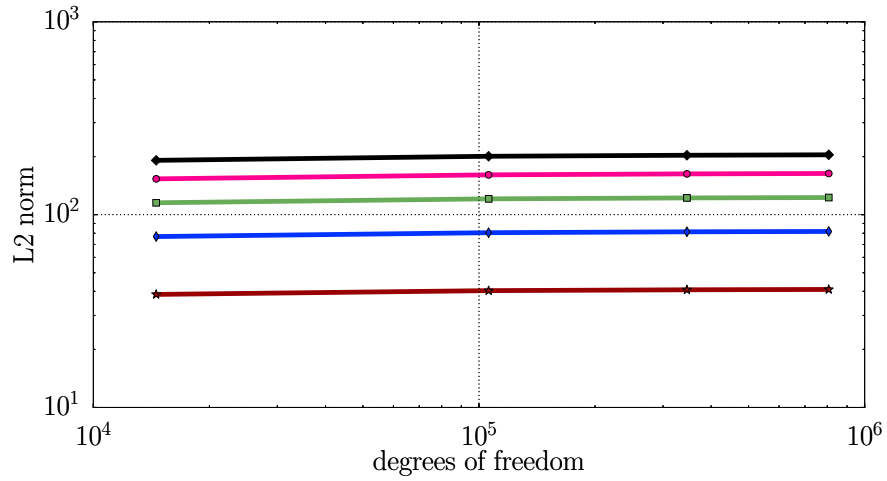
Figure 6: For the nonlinear elastic transient FEM, plot of degrees of freedom versus L_2 norm over the whole mesh in a log-log scale. Colors denote different time steps.
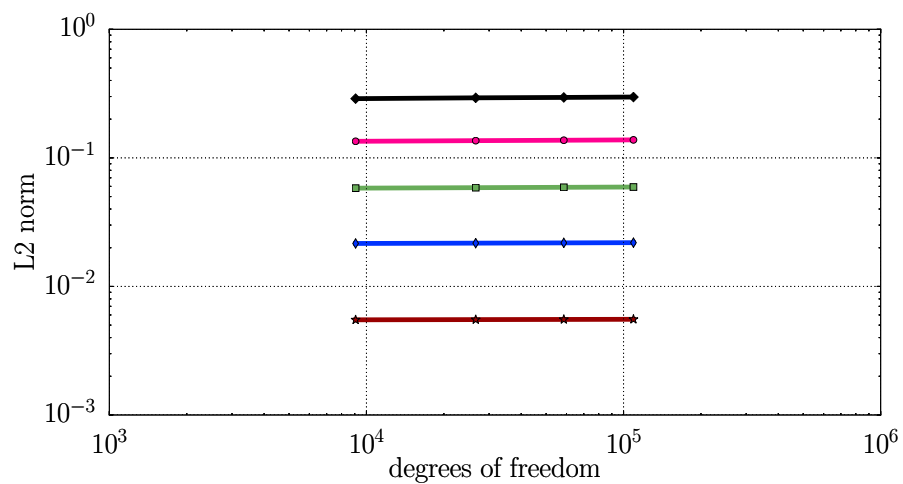

Figure 7: For the linear strain gradient elastic transient FEM, plot of degrees of freedom versus L_2 norm over the whole mesh in a log-log scale. Colors denote different time steps.

Table 3: Convergence analysis for nonlinear elastic transient FEM computation.

dofs	t_1	t_2	t_3	t_4	t_5
	L_2 norm				
14 553	38.564	76.962	115.198	153.275	191.195
105 903	40.346	80.586	120.727	160.774	200.733
346 053	40.755	81.440	122.066	162.641	203.177
807 003	40.920	81.791	122.628	163.446	204.259

Table 4: Convergence analysis for linear strain gradient elastic transient FEM computation.

dofs	t_1	t_2	t_3	t_4	t_5
	L_2 norm				
9 075	0.005499	0.021587	0.058142	0.134536	0.288832
26 607	0.005520	0.021714	0.058642	0.136126	0.293113
58 563	0.005536	0.021813	0.059021	0.137123	0.295191
109 263	0.005549	0.021895	0.059326	0.138029	0.297284

Acknowledgements

References

Abali, B. E. 2017a.
Computational Reality, Solving Nonlinear and Coupled Problems in Continuum Mechanics.
Advanced Structured Materials. Springer.

Abali, B. E. 2017b.
Technical University of Berlin, Institute of Mechanics, Chair of Continuums Mechanics and Material Theory, Computational Reality.
http://www.lkm.tu-berlin.de/ComputationalReality/.

Abali, B. E. and Müller, W. H. 2016.
Numerical solution of generalized mechanics based on a variational formulation.
Oberwolfach reports - Mechanics of Materials, European Mathematical Society Publishing House, 17(1):9–12.

Abali, B. E., Müller, W. H., and Eremeyev, V. A. 2015.
Strain gradient elasticity with geometric nonlinearities and its computational evaluation.
Mechanics of Advanced Materials and Modern Processes, 1(4).

Ahrens, J., Geveci, B., and Law, C. 2011.
ParaView: An End-User Tool for Large Data Visualization, Visualization handbook, chapter 36, pages 717–731.
Elsevier Academic Press.

Alnæs, M. S. and Mardal, K.-A. 2010.
On the efficiency of symbolic computations combined with code generation for finite element methods.
ACM Transactions on Mathematical Software (TOMS), 37(1):6.

Alnaes, M. S. and Mardal, K.-A. 2012.
  SyFi and SFC: Symbolic Finite Elements and Form Compilation, chapter 15.
  Springer.

Auffray, N., dell'Isola, F., Eremeyev, V., Madeo, A., and Rosi, G. 2015.
  Analytical continuum mechanics à la hamilton–piola least action principle for second gradient continua and
  capillary fluids.
  Mathematics and Mechanics of Solids, 20(4):375–417.

Ayachit, U. 2015.
  The paraview guide: a parallel visualization application.
  Technical report, Kitware.

Barenblatt, G. I. 1996.
  Scaling, self-similarity, and intermediate asymptotics: dimensional analysis and intermediate asymptotics,
  volume 14.
  Cambridge University Press.

Bilotta, A., Formica, G., and Turco, E. 2010.
  Performance of a high-continuity finite element in three-dimensional elasticity.
  International Journal for Numerical Methods in Biomedical Engineering, 26(9):1155–1175.

Brezny, R. and Green, D. 1990.
  Characterization of edge effects in cellular materials.
  Journal of Materials Science, 25(11):4571–4578.

Chen, C. and Fleck, N. 2002.
  Size effects in the constrained deformation of metallic foams.
  Journal of the Mechanics and Physics of Solids, 50(5):955–977.

dell'Isola, F., Andreaus, U., and Placidi, L. 2014.
  At the origins and in the vanguard of peridynamics, non-local and higher-gradient continuum mechanics: An
  underestimated and still topical contribution of gabrio piola.
  Mathematics and Mechanics of Solids, 20:887–928.

dell'Isola, F., Sciarra, G., and Vidoli, S. 2009.
  Generalized Hooke's law for isotropic second gradient materials.
  Proceedings of the Royal Society A: Mathematical, Physical and Engineering Science, 465:2177–2196.

Eremeyev, V. A. 2016.
  On equilibrium of a second-gradient fluid near edges and corner points.
  In: Advanced Methods of Continuum Mechanics for Materials and Structures, pages 547–556. Springer.

Eremeyev, V. A. and Altenbach, H. 2014.
  Equilibrium of a second-gradient fluid and an elastic solid with surface stresses.
  Meccanica, 49(11):2635–2643.

Eringen, A. 1967.
  Theory of micropolar elasticity.
  Technical report, DTIC Document.

Giorgio, I. 2016.
  Numerical identification procedure between a micro-cauchy model and a macro-second gradient model for
  planar pantographic structures.
  Zeitschrift für angewandte Mathematik und Physik, 67(4):95.

Gnu Public 2007.
  Gnu general public license.
  http://www.gnu.org/copyleft/gpl.html.

Hoffman, J., Jansson, J., Johnson, C., Knepley, M., Kirby, R., Logg, A., Scott, L. R., and Wells, G. N. 2005.
  Fenics.
  http://www.fenicsproject.org/.

Javili, A., dell'Isola, F., and Steinmann, P. 2013.
  Geometrically nonlinear higher-gradient elasticity with energetic boundaries.
  Journal of the Mechanics and Physics of Solids, 61(12):2381–2401.

Jones, E., Oliphant, T., Peterson, P., et al. 2001.
  SciPy: Open source scientific tools for Python.
  http://www.scipy.org/.

Kesler, O. and Gibson, L. J. 2002.
  Size effects in metallic foam core sandwich beams.
  Materials Science and Engineering: A, 326(2):228–234.

Langanten, H. P. and Logg, A. 2017.
  Solving PDEs in Python, volume 3 of Simula SpringerBriefs on Computing.
  Springer.

Logg, A., Mardal, K. A., and Wells, G. N. 2011.
  Automated solution of differential equations by the finite element method, the FEniCS book, volume 84 of
  Lecture Notes in Computational Science and Engineering.
  Springer.

Mindlin, R. D. 1964.
  Micro-structure in linear elasticity.
  Archive for Rational Mechanics and Analysis, 16(1):51–78.

Mindlin, R. D. 1965.
  Second gradient of strain and surface-tension in linear elasticity.
  International Journal of Solids and Structures, 1(4):417–438.

Mindlin, R. D. and Tiersten, H. F. 1962.
  Effects of couple-stresses in linear elasticity.
  Archive for Rational Mechanics and Analysis, 11:415–448.
  10.1007/BF00253946.

Morrison, J. 1939.
  The yield of mild steel with particular reference to the effect of size of specimen.
  Proceedings of the Institution of Mechanical Engineers, 142(1):193–223.

Neff, P., Ghiba, I.-D., Madeo, A., Placidi, L., and Rosi, G. 2014.
  A unifying perspective: the relaxed linear micromorphic continuum.
  Continuum Mechanics and Thermodynamics, 26(5):639–681.

Oliphant, T. E. 2007.
  Python for scientific computing.
  Computing in Science & Engineering, 9(3):10–20.

Pideri, C. and Seppecher, P. 1997.
  A homogenization result for elastic material reinforced periodically with high rigidity elastic fibres.
  Comptes Rendus de l'Academie des Sciences Series IIB Mechanics Physics Chemistry Astronomy, 8(324):475–481.

Placidi, L., Andreaus, U., Della Corte, A., and Lekszycki, T. 2015.
  Gedanken experiments for the determination of two-dimensional linear second gradient elasticity coefficients.
  Zeitschrift für angewandte Mathematik und Physik, 66(6):3699–3725.

Polizzotto, C. 2013a.
  A second strain gradient elasticity theory with second velocity gradient inertia–part i: Constitutive equations
  and quasi-static behavior.
  International Journal of Solids and Structures, 50(24):3749–3765.

Polizzotto, C. 2013b.
  A second strain gradient elasticity theory with second velocity gradient inertia–part ii: Dynamic behavior.
  International Journal of Solids and Structures, 50(24):3766–3777.

Reiher, J. C., Giorgio, I., and Bertram, A. 2016.
  Finite-element analysis of polyhedra under point and line forces in second-strain gradient elasticity.
  Journal of Engineering Mechanics, page 04016112.

Romano, G., Barretta, R., and Barretta, A. 2009.
  On maupertuis principle in dynamics.
  Reports on Mathematical Physics, 63(3):331–346.

Scerrato, D., Zhurba Eremeeva, I. A., Lekszycki, T., and Rizzi, N. L. 2016.
  On the effect of shear stiffness on the plane deformation of linear second gradient pantographic sheets.
  ZAMM-Journal of Applied Mathematics and Mechanics/Zeitschrift für Angewandte Mathematik und Mechanik, 96(11):1268–1279.

Steigmann, D. J. and dell'Isola, F. 2015.
  Mechanical response of fabric sheets to three-dimensional bending, twisting, and stretching.
  Acta Mechanica Sinica, 31(3):373–382.

Toupin, R. A. 1964.
  Theories of elasticity with couple-stress.
  Archive for Rational Mechanics and Analysis, 17(2):85–112.

Turco, E., Golaszewski, M., Cazzani, A., and Rizzi, N. L. 2016.
  Large deformations induced in planar pantographic sheets by loads applied on fibers: experimental validation of a discrete lagrangian model.
  Mechanics Research Communications, 76:51–56.

Yang, J. and Lakes, R. S. 1982.
  Experimental study of micropolar and couple stress elasticity in compact bone in bending.
  Journal of biomechanics, 15(2):91–98.